Journal of Materials Chemistry C

Accepted Manuscript

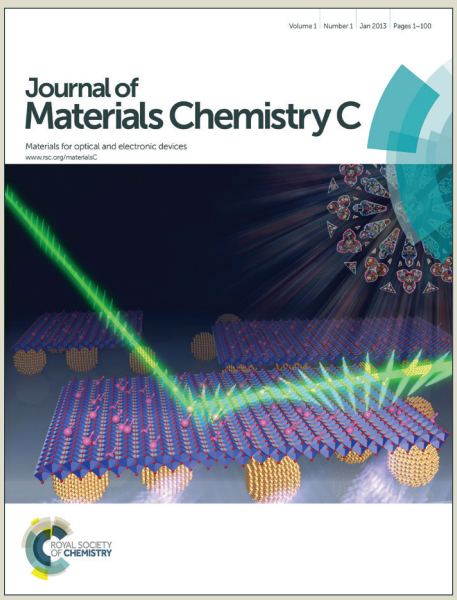

ROYAL SOCIETY OF CHEMISTRY

www.rsc.org/materialsC

Journal Name

ARTICLE

Asymmetrical twisted anthracene derivatives as high-efficiency deep-blue emitters for organic light-emitting didoes

Received 00th January 20xx,
Accepted 00th January 20xx

DOI: 10.1039/x0xx00000x

www.rsc.org/

Chuanyou He,[a] Haoqing Guo,[a] Qiming Peng,[a] Shengzhi Dong,[a] Feng Li*[a]

Deep-blue emission is particularly important for the applications of organic light-emitting diodes (OLEDs) in the full colour flat-panel displays and solid-state lighting resources. Two asymmetrical twisted anthrancene derivatives, 4,5-diphenyl-1,2-bis(4-(10-phenylanthracen-9-yl)phenyl)-1H-imidazole (DPA-PIM) and 1,2-bis(4-(10-phenylanthracen-9-yl)phenyl)-1H-phenanthro[9,10-d]imidazole (DPA-PPI), for deep-blue OLEDs have been designed and synthesized. The asymmetrical twisted conformations between anthracene and imidazole units in compounds efficiently interrupt molecular π-conjugation and inhibit π-π intermolecular interactions, resulting in a high thermal stability and an efficient deep-blue emission. The two anthrancene derivatives in non-doped OLEDs exhibited blue emission. Especially, the non-doped device based on DPA-PIM achieved an external quantum efficiency (EQE) of 6.5 % with a CIE coordinate of (0.15, 0.08). In addition, the two emitters in doped devices achieved high EQEs over 5.0 % and much purer blue emission with CIE coordinates of (0.15, 0.06) for DPA-PPI and (0.15, 0.05) for DPA-PIM, which nearly match the CIE of European Broadcasting Union (EBU) blue standard of (0.15, 0.06).

Introduction

Organic light-emitting diodes (OLEDs) have made a great progress in flat-panel displays and solid-state lighting resource over decades since the first report by C. W. Tang and Van Slyke in 1987.[1] To achieve full colour displays, three basic colours (blue, green, red) are necessary. Moreover, blue/deep-blue emitter is particularly important, because it not only acts as one of three basic colours but also generates green/red emissions though energy transfer.[2] However, the performance of blue/deep-blue OLEDs is often inferior to that of green/red OLEDs.[3] Because of that, high performance blue emitters which meet the Commission International de l'Eclairage coordinates (CIE) (x, y) = (0.15, 0.06) according to the European Broadcasting Union (EBU) standard are rare.[4]

Anthracene has been widely used as building block and starting materials for blue emitters due to its unusual photoluminescence (PL) and electroluminescence (EL) properties.[5] However, its intrinsic character of easy crystallization in solid-state film limited the applications. To suppress the troublesome crystallization and improve thermal stability, the modification of anthracene mostly concerned on replacing the substituents at its C-9 and -10 positions.[5a] One strategy for molecular design is introduction of steric hindrance and forming a non-coplanar molecular structure which could efficaciously suppress crystallization.[6] Another strategy is to introduce asymmetrical structure which might not only strengthen amorphous morphological ability, but also improve the efficiency by slightly changing the substituents.[7] In the past several years, many 9,10-disubstituted anthracene derivatives with improved thermal stability have been reported and devices utilizing them as host exhibited high efficiency.[5a] However, the non-doped devices based on anthracene derivatives usually showed broad and featureless EL spectra due to close packing in thin film and π-π intermolecular interaction from anthracene planes.[2b] Recently, some progresses[4b,8] have been made to obtain highly efficient deep-blue anthracene derivatives by introducing non-planar rotational molecular structure which efficiently interrupted the π-conjugation. Thus, the rational choose of side groups might be an important factor for designing deep-blue materials consisting of anthracene moiety.

In this work, we designed and synthesized two anthrancene derivatives, 4,5-diphenyl-1,2-bis(4-(10-phenylanthracen-9-yl)phenyl)-1H-imidazole (DPA-PIM) and 1,2-bis(4-(10-phenylanthracen-9-yl)phenyl)-1H-phenanthro[9,10-d]imidazole (DPA-PPI), as shown in Scheme 1. An imidazole ring couples with two 9,10-diphenylanthracene moieties at its N-1 and C-2 position that forms an asymmetrical twisted structure. On the one hand, high thermal stability benefits from asymmetrical twisted molecular structure. On the other hand, the π-conjugation between imidazole and 9-phenylanthracene is interrupted by the twisted benzene ring then produces deep-blue emission. In addition, the outside phenyl units are in a direction perpendicular to the anthracene planes.

[a] State Key Laboratory of Supramolecular Structure and Materials, Institute of Theoretical Chemistry, Jilin University, Qianjin Avenue 2699, Changchun, 130012, P. R. China. E-mail: lifeng01@jlu.edu.cn

† Electronic Supplementary Information (ESI) available: the details of the synthesis; the PL spectra of DPA-PPI and DPA-PIM in cycle-hexane, toluene, dichloromethane solution; the EL spectra of the DPA-PPI-based OLEDs and DPA-PIM-based OLEDs at different voltages; the energy diagram of compounds utilized in non-doped devices. See DOI: 10.1039/x0xx00000x

That geometrical morphology tends to maintain a certain distance between the anthrance units of adjacent molecules and suppress the close parking and π-π intermolecular interaction [9] Both of the anthrancene derivatives in non-doped OLEDs exhibited blue emission. Especially, the non-doped device based on DPA-PIM exhibited high external quantum efficiency (EQE) of 6.5 % with a CIE coordinate of (0.15, 0.08). Moreover, the two emitters in doped devices achieved much purer blue emission with CIE coordinates of (0.15, 0.06) for DPA-PPI and (0.15, 0.05) for DPA-PIM, which are close to the CIE of European Broadcasting Union (EBU) blue standard (0.15, 0.06).

Experimental section

General information

The Mass spectra and NMR spectra were measured with a Thermo Fisher ITQ1100 GC-MS spectrometer and Bruker AVANCEIII500 spectrometer, respectively. The elemental analysis was collected on Elementar (Vario micro cube) instrument. Differential scanning calorimetry (DSC) was recorded on Netzsch DSC204 instrument at a heating rate of 10 ^{o}C/ min from 20 to 400 ^{o}C in a nitrogen atmosphere. The thermogravimetric analysis (TGA) was performed on TA Q500 instrument. For the absorption and PL measurements, compounds were dissolved into solvent with a concentration of 1×10^{-5} mol/L, or evaporated to a quartz substrate in a high vacuum chamber with the thickness of 60 nm. Then the spectra were measured using a UV-Vis spectrophotometer (Shimadzu UV-2550) and a spectrofluorophotometer (Shimadzu RF-5301PC), respectively. The cyclic voltammetry (CV) measurements were performed using an electrochemical analyzer (CHI660C, CH Instruments, USA). A glass carbon disk served as the working electrode. A platinum wire was the auxiliary electrode with a porous ceramic wick. And Ag/Ag^{+} acted as the reference electrode, standardized for the redox couple ferricinium/ferrocene. Anhydrous N,N-dimethylformamide (DMF) and dichloromethane (CH_2Cl_2) contained 0.1 M tertrakis(n-butyl)ammonium hexafluorophosphate (NBu_4PF_6) as the supporting electrolyte were used as the solvents under a nitrogen atmosphere. A scan rate of 50 mV/s was applied.

Synthesis

The synthesis route and chemical structures of compounds are described in Scheme 1 and Electronic Supplementary Information**.** 4,4,5,5-Tetramethyl-2-(10-phenylanthracen-9-yl)-1,3,2-dioxaborolane (1a), 1,2-bis(4-bromophenyl)-1H-phenanthro[9,10-d]imidazole (1b), 1,2-bis(4-bromophenyl)-4,5-diphenyl-1H-imidazole (1c), were prepared according to literatures[10]. Compound 1a attached to compound 1b and compound 1c through Suzuki couple reaction with good yields to get final products DPA-PPI and DPA-PIM, respectively. The target compounds were purified with the silica column and characterized with ^{1}H NMR spectroscopy, ^{13}C NMR spectroscopy, mass spectrometry and elemental analysis.

Preparation of DPA-PPI. Compound 1a (3.6 g, 9.46 mmol), compound 1b (2.0 g, 3.78 mmol), and $Pd(PPh_3)_4$ (175 mg, 0.15 mmol) were mixed in a 100 mL flask containing K_2CO_3 aqueous solution (16 mL, 2 M), ethanol (8 mL) and anhydrous toluene (24 mL). The mixture was refluxed for 48 h under nitrogen. After cooled to room temperature, the reaction mixture was quenched with dilute hydrochloric acid solution and extracted with CH_2Cl_2. The organic extracts were dried over anhydrous $MgSO_4$ and concentrated by rotary evaporation. The crude product was further purified by silica gel column chromatography (CH_2Cl_2/petroleum ether (3:2,v/v)) to get DPA-PPI as light yellow powder (2.1 g, 62.9 %). ^{1}H NMR (500 MHz, CD_2Cl_2) δ 8.95 (d, *J* = 8.3 Hz, 1H), 8.87 (d, *J* = 8.3 Hz, 1H), 8.13 (d, *J* = 7.4 Hz, 2H), 8.05 – 7.98 (m, 3H), 7.88 (t, *J* = 7.6 Hz, 3H), 7.80 (d, *J* = 7.8 Hz, 5H), 7.76 – 7.57 (m, 15H), 7.56 – 7.51 (m, 4H), 7.51 – 7.45 (m, 1H), 7.41 – 7.32 (m, 4H), 7.28 – 7.23 (m, 1H), 7.15 – 7.10 (m, 1H). ^{13}C NMR (126 MHz, CD_2Cl_2) δ 138.94, 138.77, 137.97, 133.42, 131.36, 131.25, 131.20, 129.88, 129.78, 129.74, 129.57, 128.45, 127.63, 127.56, 127.20, 127.02, 126.94, 126.67, 126.32, 125.99, 125.77, 125.67, 125.35, 125.19, 125.08, 124.30, 123.31, 121.18, 118.98. EI-MS (m/z) Calculated for $C_{67}H_{42}N_2$: 875.06. Found [M^{+}]: 875.7. Elem. Anal. Calcd for $C_{67}H_{42}N_2$: C, 91.96; H, 4.84; N, 3.20. Found: C, 92.14; H, 4.82; N, 3.19.

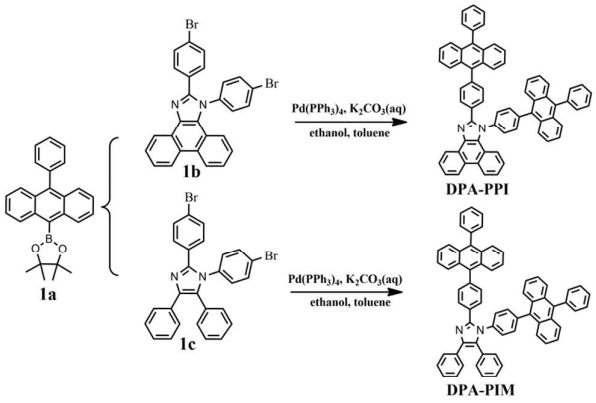

Scheme 1. The synthesis route of DPA-PPI and DPA-PIM

Preparation of DPA-PIM. The procedure was analogous to that described for DPA-PPI (54.1%, light yellow powder). ^{1}H NMR (500 MHz, CD_2Cl_2) δ 7.87 (s, 2H), 7.72 – 7.64 (m, 4H), 7.61 (dd, *J* = 6.7, 3.0 Hz, 2H), 7.58 – 7.50 (m, 7H), 7.50 – 7.45 (m, 4H), 7.44 – 7.30 (m, 14H), 7.30 – 7.10 (m, 11H). ^{13}C NMR (126 MHz, $CDCl_3$) δ 131.42, 131.32, 131.23, 129.91, 129.83, 129.79, 129.62, 128.89, 128.51, 128.43, 128.32, 127.59, 127.51, 127.15, 127.03, 126.76, 126.09, 125.50, 125.27, 125.04.EI-MS (m/z) Calculated for $C_{67}H_{42}N_2$: 877.08. Found [M^{+}]: 877.9. Elem. Anal. Calcd for $C_{67}H_{44}N_2$: C, 91.75; H, 5.06; N, 3.19. Found: C, 91.90; H, 5.07; N, 3.18.

Device fabrication and measurements

The indium tin oxide (ITO) glass substrates were cleaned with acetone, toluene, ethanol, and dichloromethane. After treated with UV irradiation for 20 min, the samples were transferred into a deposition system. The devices were fabricated by the multiple sources organic molecular beam deposition method in vacuum at a

pressure of 4×10^{-6} mbar. Evaporation rates of 0.4 Å/s for the organic materials and 1-4 Å/s for the metal electrodes were applied. The current density–voltage (J–V) characteristics were measured by a Keithley 2400 source meter. The luminance–voltage (L–V) characteristic and the EL spectrum were measured by a Photo Research spectroradiometer (PR650).

Results and discussion

Thermal properties

Thermal properties of DPA-PPI and DPA-PIM were investigated by thermogravimetric analysis (TGA) and differential scanning calorimetry (DSC). As shown in Figure 1a, a decomposition temperature (T_d, corresponding to 5 % weight loss) of 550 °C for DPA-PPI was obtained owing to the large rigid plane of phenanthro[9,10-d]imidazole. Compared to DPA-PPI, the more flexible molecular structure of DPA-PIM shows relatively poor thermal stability with a T_d of 480 °C (Figure 1b). In addition, no obvious glass transition and endothermic melting transition were observed for DPA-PPI and DPA-PIM. This means that amorphous film can be gained after vacuum deposition. And the detail data was summarized in Table 1. The results confirm that the imidazole ring coupled with 9,10-diphenylanthracene moieties at its N-1 and C-2 positions to form an asymmetric twisted structure could greatly improve thermal stability, which is important for the application in devices.

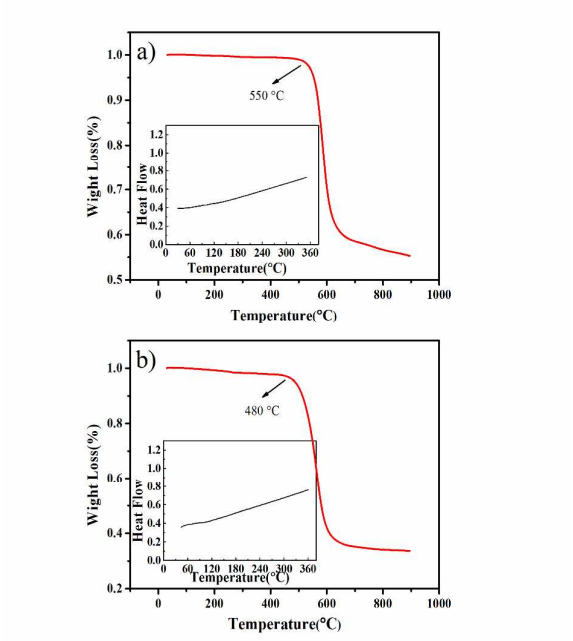

Figure 1. TGA and DSC (the inset) curves for DPA-PPI (a) and DPA-PIM (b).

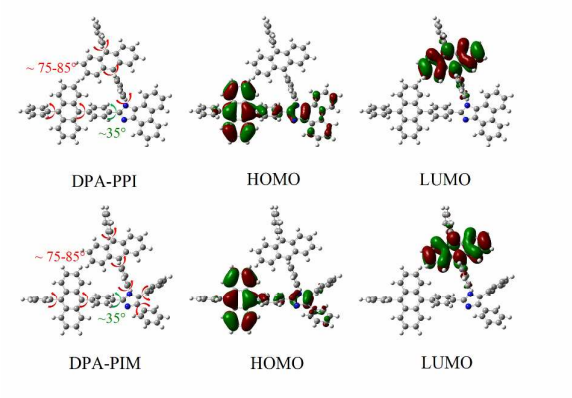

Figure 2. The optimized molecular geometry and the calculated HOMO and LUMO density maps of DPA-PPI (top) and DPA-PIM (down) at B3LYP/6-31G (d) level.

Theoretical Calculation

Density functional theory (DFT) calculations (B3LYP) were performed for DPA-PPI and DPA-PIM with 6-31G (d) basis set by using Gauss 09 program. The optimized molecular geometry and the calculated highest occupied molecular orbital (HOMO) and lowest unoccupied molecular orbital (LUMO) density maps are shown in Figure 2. From the optimized molecular geometry, the π-conjugation between imidazole and 9-phenylanthracene is interrupted by the twisted benzene ring that could induce blue emission. Besides, the outside phenyl units bind anthracene in a

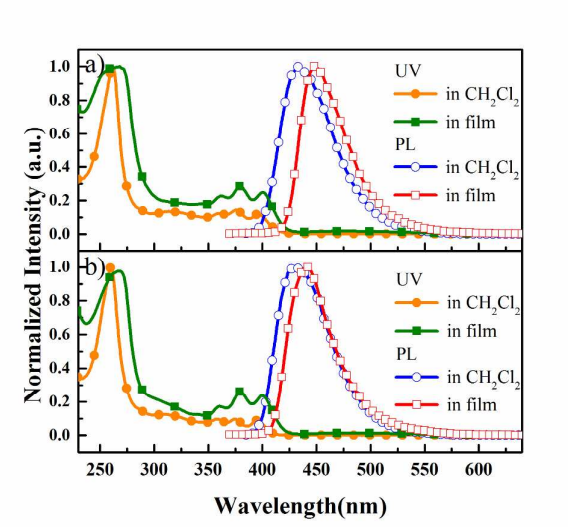

Figure 3. The UV-vis absorption spectra (solid symbols) and PL spectra (open symbols) in CH_2Cl_2 solution (circle) and thin film (square) of DPA-PPI (a) and DPA-PIM (b).

Table 1. Physical data of compounds.

	DPA-PPI	DPA-PIM
T_d/T_g (°C)	550/-	480/-
$\lambda_{abs.}$ [a] (nm)	360/375/396	360/375/396
$\lambda_{abs.}$ [b] (nm)	362/380/400	362/380/400
λ_{PL} [a]/ λ_{PL} [b] (nm)	433/448	428/441
Φ_F	~1[c] (0.11)[d]	0.78[c] (0.09)[d]
HOMO/LUMO (eV)[e]	-5.56/-2.55	-5.58/-2.53
E_g [e] (eV)	3.01	3.05

[a] CH_2Cl_2 solution (room temperature); [b] neat film; [c] in CH_2Cl_2 using quinine sulphate as standard; [d] in film using an integrating sphere photometer; [e] calculated by comparing with ferrocene (Fc) and calibrated using $E_{1/2}$(Fe/Fe+) =0.20V.

direction perpendicular that tends to inhibit the π-π intermolecular interaction. The shapes of HOMO and LUMO orbitals of DPA-PPI and DPA-PIM are almost same. The LUMO is located on the anthrancene unit at the N-1 position of imidazole ring. The HOMO is mainly localized on the imidazole group and the anthrancene unit at the C-2 position of imidazole ring.

Optical properties

We collected the UV-vis absorption and PL spectra of DPA-PPI and DPA-PIM in dilute CH_2Cl_2 solution (10^{-5} mol/L) and thin film state to evaluate their optical properties as shown in Figure 3**.** The key photophysical data is summarized in Table 1. DPA-PPI and DPA-PIM show similar absorption peaks both in CH_2Cl_2 solution and in thin film. A higher intensity absorption peak around 260 nm can be seen

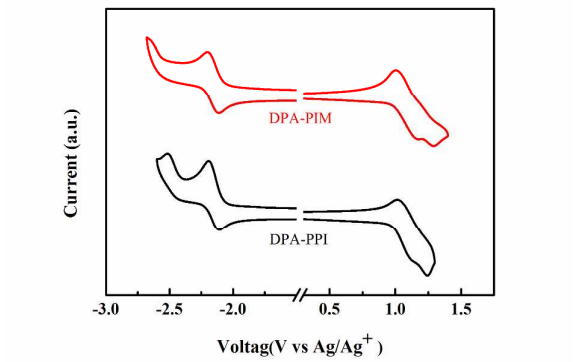

Figure 4. Cyclic voltammograms of DPA-PPI (black) and DPA-PIM (red)

which originates from the π-π* transition of the benzene ring. Three lower intensity absorption bounds around 360, 375, 395 nm are attributed to the π-π* transition of anthracene. For the PL spectra, both DPA-PPI and DPA-PIM exhibit deep-blue emission in CH_2Cl_2 solution. The maximum emission wavelengths of DPA-PPI and DPA-PIM are at 433 nm and 428 nm, respectively. While the emission peaks in film state are red-shifted by 15 nm for DPA-PPI and 13 nm for DPA-PIM compared with those of solution in CH_2Cl_2. Due to the more twisting molecular structure, the PL spectra of DPA-PIM exhibit hypochromatic shift in comparison with those of DPA-PPI. It should be noted that using 9,10-diphenylanthracene units to substitute on the N-1 and C-2 positions of imidazole can efficiently limit the π conjugation, which induces the deep-blue emission. In addition, a slight red-shift can be observed from the PL spectra in cycle-hexane, toluene, and dichloromethane for DPA-PPI and DPA-

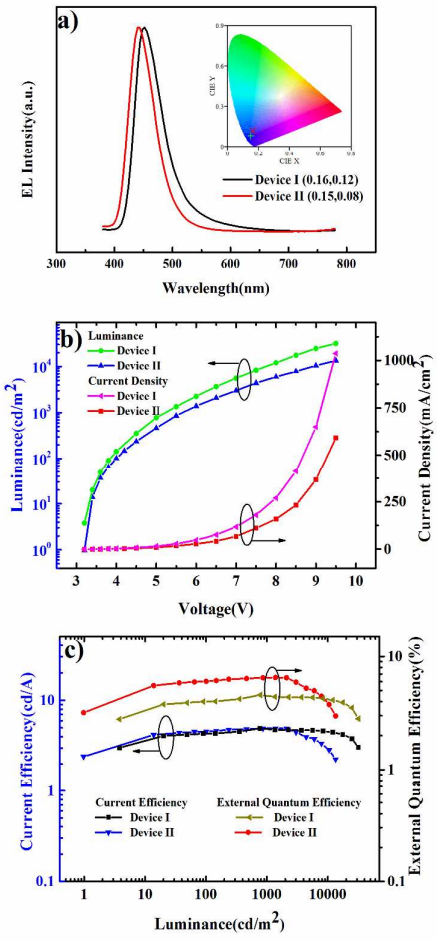

Figure 5. a) The EL spectra of DPA-PPI (Device I) and DPA-PIM (Device II) at 5V; b) the current density-voltage-luminance characteristics of non-doped devices (Device I and Device II); c) the current efficiency and the external quantum efficiency of the OLEDs.

PIM (Figure S1 and S2). The PL quantum yield (Φ_F) of DPA-PPI was determined as high as nearly 1, using quinine sulphate as the standard.[11] A lower Φ_F with a value of 0.78 for DPA-PIM was collected, owing to the more flexible molecular structure.

Electrochemical properties

The HOMO and LUMO energy levels of the two compounds were measured by cyclic voltammetry (CV). As shown in Figure 4, the cyclic voltammograms of DPA-PPI and DPA-PIM are similar. From the onset of the oxidation curves, the HOMO levels were estimated to be -5.56 eV and -5.58 eV for DPA-PPI and DPA-PIM, respectively, by using ferrocene as the reference. And from the onset of reduction curves, the LUMO levels were estimated to be -2.55 eV for DPA-PPI and -2.53 eV for DPA-PIM. The band gap of DPA-PPI and DPA-PIM can be calculated to be 3.01 eV and 3.05 eV, respectively.

Electroluminescence properties

Initially, we investigated the performance of non-doped devices based on DPA-PPI (Device I) and DPA-PIM (Device II). The device structure was optimized to be: ITO/ MoO_3 (5 nm)/ N,N′-bis(1-naphthyl)-N,N′-diphenyl-1,1′-biphenyl- 4,4′-diamine (NPB, 25 nm)/ 4,4′,4″-tri(N-carbazolyl)-triphenylamine (TCTA, 10 nm) / DPA-PPI or DPA-PIM (20 nm)/ 1,3,5-tris(N-phenylbenzimidazol-2-yl)benzene (TPBI, 50 nm)/ LiF (0.7 nm)/ Al (100 nm). Here MoO_3 and LiF were utilized as a hole-injection layer and an electron-injection layer, respectively. NPB acted as a hole-transporting layer. TCTA was used as an electron-blocking layer. TPBI was the electron-transporting and hole-blocking layers. As shown in Figure 5a, both the non-doped devices show blue emission. And the EL spectra of the devices barely change over the whole voltages ranging from 3.5 V to 9 V (Figure S3 and S4). The performance of all devices is summarized in Table 2. The device based on DPA-PPI achieves a high luminance of 31688 cd/m^2. Device I exhibits a maximum current efficiency (CE) of 4.9 cd/A and a maximum external quantum efficiency (EQE) of 4.6 % under 770 cd/m^2. Comparing to DPA-PPI, the device using DPA-PIM as blue emitters shows a purer blue emission with a CIE coordinate of (0.15, 0.08) which could be attributed to the fully twisted molecular structure. Device II shows a lower luminance of 13408 cd/m^2 and a maximum CE of 4.9 cd/A. In addition, the maximum EQE of Device II is up to a value of 6.5 %. The performance of non-doped devices indicates that asymmetrical twisted molecular structure can efficiently suppress the π-π intermolecular interaction between adjacent molecules and result in pure deep-blue emission. A slight roll-off on the efficiency is obtained as brightness or current density increase in Figure 5c. Under luminance value of 100 cd/m^2, 1000 cd/m^2 and 10000 cd/m^2, the device based on DPA-PPI (DPA-PIM) shows high EQE of 4.0 % (6.0%), 4.5 % (6.5%) and 4.2 % (4.1%), respectively. As shown in Figure S7, there are small energy barriers between emitters and charge-transporting materials. The slight roll-off on efficiency might benefit from the balanced hole and electron injection and transport.

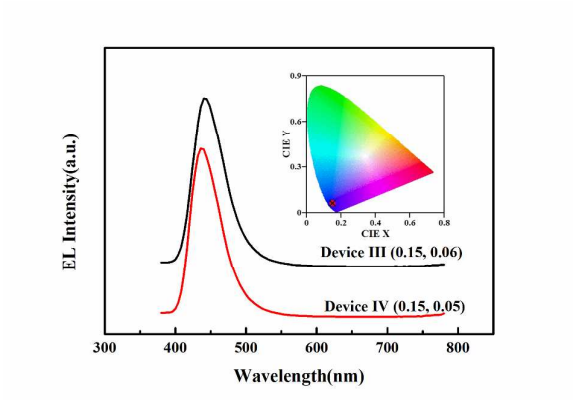

Figure 6. The EL spectra of DPA-PPI (Device III) and DPA-PIM (Device IV) doped in CBP at 5V. Inset: the CIE coordinates of the EL spectra of Device III (red dot) and Device IV (black cross).

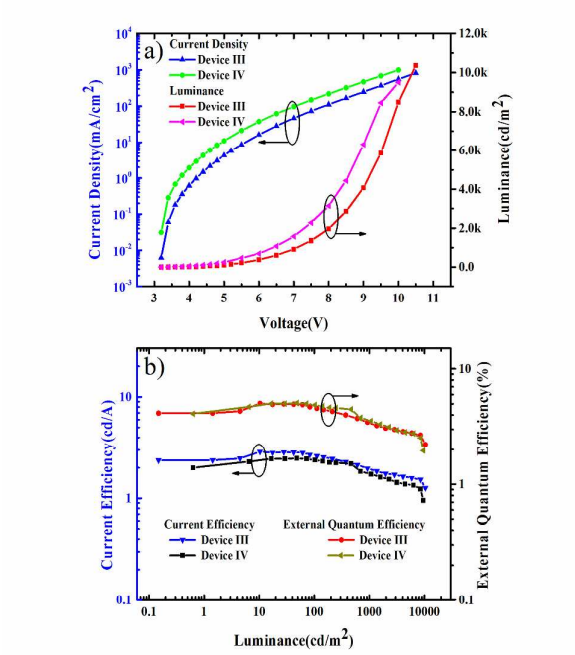

Figure 7. a) The current density-voltage-luminance characteristics of the doped devices (Device III and Device IV); b) The current efficiency and the external quantum efficiency of the OLEDs.

To further explore the electroluminescence properties of DPA-PPI and DAP-PIM, doped devices were fabricated where DPA-PPI and DAP-PIM were doped into CBP. The optimized devices structures are: ITO/ MoO_3 (5 nm)/ TCTA (40 nm)/ DPA-PPI (Device III) or DPA-

PIM

Table 2. The performance of devices.

	V_{on} [a]	λ_{max} [b]	L_{max} [c]	$CE_{max/100/1000}$ [d]	$EQE_{max/100/1000}$ [e]	CIE
	[V]	[nm]	[cd m^{-2}]	[cd A^{-1}]	[%]	(x,y)
Device I	3.2	452	31688	4.9/2.6/2.9	4.6/4.0/4.5	(0.16,0.12)
Device II	3.2	444	13408	4.9/3.1/3.4	6.5/6.0/6.5	(0.15,0.08)
Device III	3.2	440	10369	2.9/2.4/1.9	5.0/4.6/3.4	(0.15,0.06)
Device IV	3.2	436	9505	2.5/2.3/1.7	5.1/4.9/3.6	(0.15,0.05)

[a]Turn-on voltage; [b]the maximum EL wavelength; [c] the maximum Luminance; [d] the maximum/ at 100 cd/m^2/at 1000 cd/m^2; [e] the maximum/ at 100 cd/m^2/ at 1000 cd/m^2.

(Device IV): 4,4'-Bis(N-carbazolyl)-1,1'-biphenyl (CBP, 6 wt%, 20nm)/ TPBI (50 nm)/ LiF (0.7 nm)/ Al (100 nm), where CBP was used as the host and TCTA was used as the hole-transporting layer. The EL spectra of the two devices at 5 V are shown in Figure 6. As can been seen, both of the resulting spectra show deep-blue emission peaks around 440 nm for DPA-PPI and 436 nm for DPA-PIM with a FWHM of 50 nm. More specifically, the CIE coordinates of (0.15, 0.06) for DPA-PPI and (0.15, 0.05) for DPA-PIM perfectly meet the EBU blue standard of (0.15, 0.06). Device III achieves a maximum luminance of 10369 cd/m^2, a maximum CE of 2.9 cd/A and a maximum EQE of 5.0 %. Moreover, Device IV shows a similar performance with a maximum CE of 2.5 cd/A and a maximum EQE of 5.1 %, which among the best values of deep-blue OLEDs with CIE_y ≤0.06.[2a, 4a-4d,8b,12.]

In dye-doped (guest-host system) OLEDs, there are two paths for the generation of excited state of dopant: one is energy transfer (ET);[13] another is charge trapping (CT).[14] The ET is that the excitions are formed in host followed by energy transfer to the guest through Förster and/or Dexter mechanisms.[13] Efficient energy transfer requires that the absorption spectrum of dopant overlaps significantly with the emission spectrum of a host. CT is that the excitons are directly formed in guest by trapping carriers [14] rather than acquiring energy from host excitons. It is most favourable if the LUMO energy level of the guest is lower enough than that of the host and the HOMO energy level of the guest is higher enough than that of the host.[15] In our work, the HOMO and LUMO of CBP are -6.2 eV and -2.6 eV, respectively. From Table 1 the HOMO levels of DPA-PPI and DPA-PIM are 0.64 eV and 0.62 eV above that of CBP, respectively, implying that holes are subsequently trapped on the blue dyes. Therefore, electrons can efficiently hop onto $DPA\text{-}PPI^+$ or $DPA\text{-}PIM^+$ to form excitons.

Conclusions

Two blue-light-emitting asymmetrical twisted molecules, DPA-PPI and DPA-PIM, with a imidazole ring coupled with two 9,10-diphenylanthracene moieties at its N-1 and C-2 positions have been designed and synthesized. Both DPA-PPI and DPA-PIM exhibited high thermal stabilities and deep-blue fluorescence. The non-doped devices based on the two emitters showed blue emissions and high efficiency. Especially, with the DPA-PIM as an emitter, the non-doped devices exhibited a CE up to 4.9 cd/A and a maximum EQE of 6.5% with a CIE coordinate of (0.15, 0.08). In addition, using DPA-PPI and DPA-PIM as dopants, the devices achieved a high EQE of 5.0 % (2.9 cd/A) and 5.1 % (2.5 cd/A) with CIE coordinates of (0.15, 0.06) and (0.15, 0.05), respectively, which almost meet the EBU blue standard of (0.15, 0.06).

Acknowledgements

We are grateful for financial support from the National Natural Science Foundation of China (grant numbers 61275036, 2015CB655003, 21221063 and 91233113).

Notes and references

1 C. W. Tang and S. A. VanSlyke, *Appl. Phys. Lett.*, 1987, **51**, 913.

2 (a) X. Yang, X. Xu and G. Zhou, *J. Mater. Chem. C*, 2015; (b) M. Zhu and C. Yang, *Chem. Soc. Rev.*, 2013, **42**, 4963-4976.

3 (a) S. H. Kim, I. Cho, M. K. Sim, S. Park and S. Y. Park, *J.Mater. Chem.*, 2011, **21**, 9139; (b) S. K. Kim, Y. I. Park, I. N. Kang and J. W. Park, *J. Mater. Chem.*, 2007, **17**, 4670.

4 (a) J. Y. Hu, Y. J. Pu, F. Satoh, S. Kawata, H. Katagiri, H. Sasabe and J. Kido, *Adv. Funct. Mater.*, 2013, **24**, 2064-2071; (b) R. Kim, S. Lee, K. H. Kim, Y. J. Lee, S. K. Kwon, J. J. Kim and Y. H. Kim, *Chem.Commun.*, 2013, **49**, 4664-4666; (c) Y. Yuan, J. X. Chen, F. Lu, Q. X. Tong, Q. D. Yang, H. W. Mo, T. W. Ng, F. L. Wong, Z. Q. Guo, J. Ye, Z. Chen, X. H. Zhang and C. S. Lee, *Chem. Mater.*, 2013, **25**, 4957-4965; (d) Z. Gao, Y. Liu, Z. Wang , F. Shen, H. Liu, G. Sun, L. Yao, Y. Lv, P. Lu and Y. Ma, *Chem. Eur. J.*, 2013, **19**, 2602-2605; (e) C. C. Wu, Y. T. Lin, K. T. Wong, R. T. Chen and Y. Y. Chien, *Adv. Mater.*, 2004, **16**, 61-65.

5 (a) J. Huang, J. H. Su and H. Tian, *J. Mater. Chem.*, 2012, **22**, 10977; (b) J. Huang, J. H. Su, X. Li, M. K. Lam, K. M. Fung, H. H. Fan, K. W. Cheah, C. H. Chen and H. Tian, *J. Mater. Chem.*, 2011, **21**, 2957; (c) J. K. Park, K. H. Lee, S. Kang, J. Y. Lee, J. S. Park, J. H. Seo, Y. K. Kim and S. S. Yoon, *Org. Electron.*, 2010, **11**, 905-915; (d) P. I. Shih, C. Y. Chuang, C. H. Chien, E. W. G. Diau and C. F. Shu, *Adv. Funct. Mater.*, 2007, **17**, 3141-3146.

6 (a) J. Shi and C. W. Tang, *Appl. Phys. Lett.*, 2002, **80**, 3201; (b) L. Wang, W. Y. Wong, M. F. Lin, W. K. Wong, K. W. Cheah, H. L. Tamb and C. H. Chen, *J. Mater. Chem.*, 2008, **18**, 4529–4536; (c) S. K. Kim, B. Yang, Y. Ma, J. H. Lee and J. W. Park, *J. Mater. Chem.*, 2008, **18**, 3376; (d)C.-H. Chien, C.-K. Chen, F. M. Hsu, C. F. Shu, P. T. Chou and C. H. Lai, *Adv. Funct. Mater.*, 2009, **19**, 560-566.

7 (a) K.R. Wee, W.S. Han, J.E. Kim, A.L. Kim, S. Kwon, S.O. Kang, *J. Mater. Chem.* 2011, **21**(4), 1115-23; (b) J. H. Huang, J. H. Su, X. Li, M. K. Lam, K. M. Fung, H. H. Fan, K. W. Cheah, C. H. Chen, H. Tian, *J. Mater. Chem.*2011; **21**: 2957-64.

8 (a) H. Park, J. Lee, I. Kang, H. Y. Chu, J. I. Lee, S. K. Kwon and Y. H. Kim, *J. Mater. Chem.*, 2012, **22**, 2695-2700; (b) W. Li, L. Yao, H. Liu, Z. Wang, S. Zhang, R. Xiao, H. Zhang, P. Lu, B. Yang and Y. Ma, *J. Mater. Chem. C*, 2014, **2**, 4733. (c) S. Zhuang, R. Shangguan, H. Huang, G. Tu, L. Wang and X. Zhu, *Dyes Pigments*, 2014, **101**, 93-102. (d) G. Mu, S. Zhuang, W. Zhang, Y. Wang, B. Wang, L. Wang and X. Zhu, *Org. Electron.,* 2015, **21**, 9-18

9 H. Fukagawa, T. Shimizu, N. Ohbe, S. Tokito, K. Tokumaru and H. Fujikake, *Org. Electron.*, 2012, **13**, 1197-1203.

10 (a) J. Y. Hu, Y. J. Pu, Y. Yamashita, F. Satoh, S. Kawata, H. Katagiri, H. Sasabe and J. Kido, *J. Mater. Chem. C*, 2013, **1**, 3871; (b) Z. M. Wang, P. Lu, S. Chen, Z. Gao, F. Shen, W. Zhang, Y. Xu, H. S. Kwok and Y. Ma, *J. Mater. Chem.*, 2011, **21**, 5451–5456.

11 W. H. Melhuish, *J. Phys. Chem.*, 1961, **65 (2)**, 229–235

12 (a) J. Ye, Z. Chen, M.-K. Fung, C. Zheng, X. Ou, X. Zhang, Y. Yuan and C. S. Lee, *Chem. Mater.*, 2013, **25**, 2630-2637; (b) W. Y. Hung, L. C. Chi, W. J. Chen, Y. M. Chen, S. H. Chou and K. T. Wong, *J. Mater. Chem.*, 2010, **20**, 10113.

13 (a) T. Förster, *Ann. Phys*, 1948, **437**, 55; (b) D. L. Dexter, *J. Chem. Phys.*, 1953, **21**, 836.

14 H. Suzuki and S. Hoshino, *J. Appl. Phys.*, 1996, **79**, 8816.

15 (a) Q. Peng, N. Gao, W. Li, P. Chen, F. Li and Y. Ma, *Appl. Phys. Lett.*, 2013, **102**, 193304; (b) X. Gong, J. C. Ostrowski, D. Moses, G. C. Bazan and A. J. Heeger, *Adv. Funt. Mater.*, 2003, **13**,439-444**.**